Molecular Dynamics Simulation Study of Self-Assembled Monolayers of Alkanethiol Surfactants on Spherical Gold Nanoparticles†

Pradip Kr. Ghorai‡ and Sharon C. Glotzer*,‡,§

Department of Chemical Engineering and Department of Material Science and Engineering, University of Michigan, Ann Arbor, MI 48109

Received: June 14, 2007

Atomistic molecular dynamics (MD) simulations of self-assembled alkanethiol monolayers are performed to investigate the ligand shell organization of homoligand surfactants on spherical gold nanoparticle surfaces as a function of temperature, nanoparticle size, and ligand tail length. At high temperature, we show that the ligands orient randomly with respect to the surface normal with a small tilt angle. As the temperature decreases, the molecules order and adopt a larger tilt angle. The effects of alkanethiol tail length and nanoparticle size on the tilt structure are also significant. At low temperature, we find the equilibrium conformation of alkanethiols obeys the crystallographic model, whereas at high temperature the continuous model is valid. The dependence of tilt angle on different parameters and comparison with self-assembled monolayers on flat surfaces are also discussed.

1. Introduction

Self-assembled monolayers (SAMs) of long chain molecules adsorbed via their head groups on solid substrates are an active area of research.[1−5] Such molecular assembly provides an approach for fabricating tunable surfaces with well-defined size, shape, and composition. Alkanethiol SAMs have broad application in chemical,[6,7] optical,[8,9] electronic,[10] medicine,[11] microfabrication,[12,13] and biological fields,[14,15] because their properties can be modified by selectively changing specific functional groups (head or tail groups) while keeping the entire chain conformation unchanged. For example, changing the tail groups [from CH_3 to OH] of an alkanethiol [$SH-(CH_2)_n-CH_3$] monolayer, it is possible to vary the chemical surface from hydrophobic to hydrophilic.

SAMs can be formed on various solid substrates such as gold, silver, and silicon by spontaneous adsorption of molecules from solution.[16] To date, alkanethiol SAMs on the Au(111) surface are the most widely studied because gold can be handled in ambient conditions. SAMs of hydrocarbon chains are the simplest ideal model system of biological membranes and biocompatible materials.[17,18] Recently, monolayer-protected metal nanoparticles (NPs) have been used in a variety of fields[14,15,19−22] due to their unique electronic and optical properties. The ligand shell that forms a protecting monolayer (alkanethiol SAM) around the NPs confers many interesting properties, for example, solubility in many solvents,[23] electron-transfer efficiency,[24] electrochemical charging,[25] sensing of biomolecules,[14] etc. Understanding the structure of alkanethiol SAMs on NPs and other surfaces is therefore of interest.

Previous experimental and theoretical studies of 13-carbon alkanethiol SAMs on flat gold substrates showed that the molecules adopt on average a tilt angle of $30 \pm 10°$ with respect to the surface normal at 300 K.[1,2] The tilt angle on flat silver substrates is much smaller than on gold substrates,[26] indicating the importance of substrate properties. Here we present the first computational study of ligand shell organization on spherical NP surfaces. We perform atomistic molecular dynamics (MD) simulations of alkanethiol SAMs on gold nanoparticles and show that the average tilt angle of alkanethiol chains on NP surfaces is large compared to flat substrates. We also show that the tilt angle and ligand organization on spherical surfaces strongly depend on temperature, molecular chain length, and nanoparticle core diameter.

2. Methodology

2.1 Model. We use standard force fields from the literature to model the SAM/NP systems. The total conformational energy (V_{total}) of the alkanethiol chain is given by

$$V_{total} = V_{intra} + V_{inter} \quad (1)$$

Here, V_{intra} represents the bonded interactions that arise from bond stretching (V_{bond}), bond bending (V_{angle}), and torsion ($V_{dihedral}$):

$$V_{intra} = V_{bond} + V_{angle} + V_{dihedral} \quad (2)$$

where

$$V_{bond} = \sum_{ij} K_{ij}^{r}(r_{ij} - r_{ij}^{eq})^2 \quad (3)$$

$$V_{angle} = \sum_{ijk} K_{ijk}^{\theta}(\theta_{ijk} - \theta_{ijk}^{eq})^2 \quad (4)$$

and

$$V_{dihedral} = \sum_{ijkl} a_1(1 + cos(\phi_{ijkl})) + a_2(1 + cos(2\phi_{ijkl})) + a_3(1 + cos(3\phi_{ijkl})) \quad (5)$$

† Part of the "Keith E. Gubbins Festschrift".

* Corresponding author. E-mail: sglotzer@umich.edu.
‡ Department of Chemical Engineering.
§ Department of Material Science and Engineering.

10.1021/jp0746289 CCC: $37.00
Published on Web 10/04/2007

TABLE 1: Force Field Parameters[27−30]

bond	r_{ij}^{eq} (Å)	K_{ij}^{r}[kcal/(mol/Å^2]
	bond stretch	
S−CH_2	1.81	222
CH_2-CH_2	1.54	260
CH_2-CH_3	1.54	260

angle	θ_{ijk}^{eq} (Å)	K_{ij}^{θ} [kcal/(mol/rad^2]
	angle bend	
S−CH_2−CH_2	114.4	62.5
CH_2-CH_2-CH_2	109.47	63.0
CH_2−CH_2−CH_3	109.47	63.0

dihedral	a_1 (kcal/mol)	a_2 (kcal/mol)	a_3 (kcal/mol)
	torsion		
S−CH_2−CH_2− CH_2	1.4119	−0.27187	3.147029
CH_2−CH_2−C_2−CH_2	1.4119	−0.27187	3.147029
CH_2−CH_2−C_2−CH_3	1.4119	−0.27187	3.147029

atom	σ (Å)	ϵ (kcal/mol)
	nonbonded interaction (LJ)	
S	4.25	0.39743
CH_2	3.905	0.118
CH_3	3.905	0.175
Au	2.935	0.039

atoms	D_e (kcal/mol)	r_e (Å)	α (Å^{-1})
	Au−S interaction (Morse)		
Au−S	8.763	2.65	1.47

Here r_{ij} is the bond distance between two atoms i and j and r_{ij}^{eq} is the equilibrium bond length. θ_{ijk} defines the angle between three atoms i, j, and k and θ_{ijk}^{eq} is the equilibrium angle. The four atoms i, j, k, and l define a dihedral angle ϕ_{ijkl}. K_{ij}^{r}, K_{ijk}^{θ}, a_1, a_2, and a_3 are constants.

V_{inter} is the nonbonded interaction that we model in terms of a short-range 6−12 Lennard-Jones (LJ) potential for head−head, head−tail, and tail−tail interactions and the pairwise additive Morse potential for the Au-head group (sulfur) interaction.[27] The LJ pair potential is defined by

$$V_{\text{inter}} = \sum_{ij} 4\epsilon_{ij}\left[\left(\frac{\sigma_{ij}}{r_{ij}}\right)^{12} - \left(\frac{\sigma_{ij}}{r_{ij}}\right)^{6}\right] \quad (6)$$

where σ_{ij}, ϵ_{ij}, and r_{ij} are, respectively, the atomic diameter, well depth, and distance between two interacting atoms i and j. The LJ potential is truncated and shifted smoothly to zero at a cutoff radius of r_c:

$$V_{\text{inter}}(r) = V_{\text{inter}}(r) - V_{\text{inter}}(r_c) - (r - r_c)\frac{dV_{\text{inter}}}{dr}|_{r=r_c} \quad (7)$$

The Morse potential is defined by

$$V_{\text{Morse}}^{\text{Au-S}} = D_e exp[-\alpha(r - r_e)]exp[-\alpha(r - r_e)] - 2 \quad (8)$$

where r is the distance between surface Au atoms and sulfur head groups, and D_e, r_e, and α are empirical parameters. All the interaction parameters, listed in Table 1, are taken from the literature.[27−30] We use the Lorentz−Berthelot combination rules[31] for the cross-interaction parameters.

2.2. Simulation Details. We perform MD simulations in the canonical ensemble (constant number of ligands N, volume V, and temperature T) for SAMs of alkanethiols (e.g., SH−$(CH_2)_n$−CH_3, n varies from 4 to 20) adsorbed on a flat Au(111) surface and a gold nanosphere. The details of the adsorption process of alkanethiols on solid surfaces are not well understood, but it is assumed that the hydrogen from the SH head group is lost at some stage in its association with the surface.[30,32] Experimentally it was found that in the case of alkanethiol based SAMs on a gold surface, the sulfur head groups form a $(\sqrt{3} \times \sqrt{3})R30°$ two-dimensional triangular lattice with a surface density of 21.6 Å^2 per chain.[33] In our simulations on flat surfaces as well as on spherical NP surfaces, the sulfur surface density is identical to this value. For flat surfaces, $N = 720$ surfactants and for nanospheres, different diameters of the nanoparticles (3, 4, 5, 7, and 11 nm) are simulated with fixed sulfur (head group) density (21.6 Å^2 per chain). We use the united atom model for the CH_2 and CH_3 groups. We use a cutoff radius of 10 Å. A Nose−Hoover thermostat is used to keep the system temperature constant at the desired temperature throughout the simulations. A time step of 2.0 fs is used for integrating the equations of motion, which yield good conservation of both energy and linear momentum. The equilibration is performed over a duration of 10 ns. Different properties are computed from the configurations stored at intervals of 10 ps from a production run of 10 ns. Periodic boundary conditions are used for the flat surface in the x and y directions. The distance between the gold surface and the sulfur head group (d_{Au-S}) of the alkanethiol is held constant throughout the simulations. We set $d_{Au-S} = 2.38$ Å.[34] For the Au(111) surface, the velocities of the sulfur atoms are set to zero along the z-direction (perpendicular to the xy plane). The gold NP is treated as a perfect sphere. All simulations are carried out using a slightly modified version of the DL_POLY molecular simulation package.[35] The results presented in this paper required ∼1000 CPU hours on two Apple G5 2.0 GHz processors.

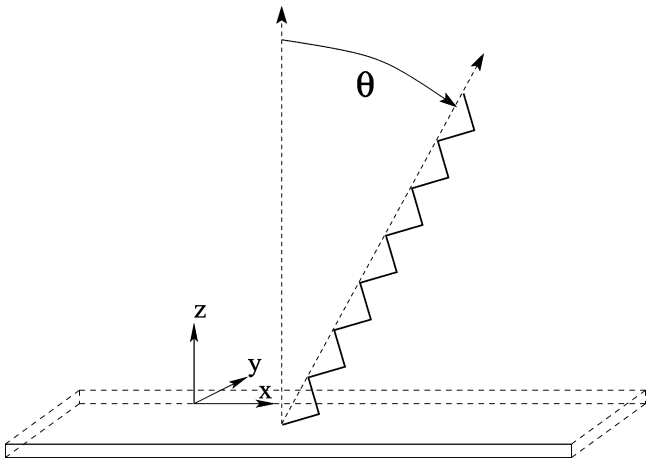

Figure 1. Schematic representation of tilt angle θ for an alkanethiol on a flat surface.

2.3. Initialization. To model the gold NPs, Au atoms are initially assigned in a random close-packed configuration on the surface of a sphere at a surface density of 10.4 Å^2/Au atom. We then relax the system at 0 K to optimize the initial structures. The carbon chains are initialized in the trans configuration, perpendicular to the surface with their sulfur head groups randomly distributed on the surface. The backbone planes of the molecules are also randomly oriented. All atoms are assigned random initial velocities according to the Maxwell−Boltzmann distribution corresponding to the target temperature. We then run the system for 10 ns until it equilibrates and the chains adopt an equilibrated tilt angle. For flat surface studies, we use similar starting configurations. In these studies, we define tilt angle as follows. On a flat surface, the tilt angle θ of the molecule is defined as the angle of the alkanethiol chain backbone with respect to the surface normal (Figure 1). On a spherical surface, the tilt angle is defined as the angle between two vectors: (i) a

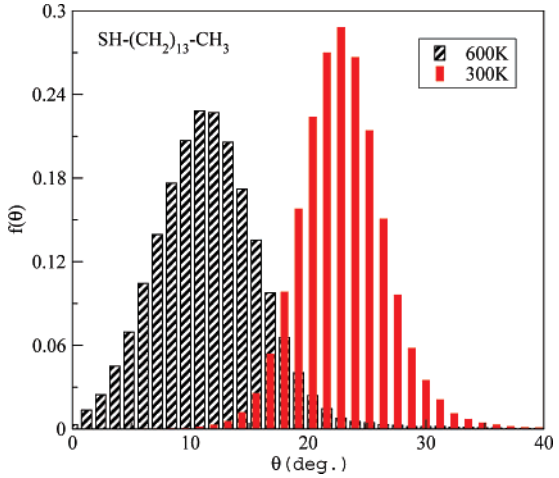

Figure 2. Distribution of tilt angle for 13-carbon alkanethiols on a Au(111) surface at 300 (rightmost data) and 600 K (leftmost data).

Figure 3. Snapshots of alkanethiol [SH−$(CH_2)_{13}$−CH_3] SAMs from our MD simulations at (a) 300 and (b) 600 K.

vector connecting the sulfur head group and the odd carbons of the alkane chain and (ii) a vector perpendicular to the surface of the sphere and passing through the sulfur head group. The tilt angle of a given chain is computed by averaging over all time steps and odd carbons.

3. Results and Discussion

3.1. Alkanethiol SAMs on Flat Au(111) Surfaces. To validate the model and force field used, we first simulate the alkanethiol SAMs on a flat Au(111) surface and compute the experimentally known tilt angle of the molecule. Figure 2 shows the tilt angle distribution for 13-carbon alkanethiols on a Au(111) surface at 300 and 600 K. We observe an average tilt angle of 24 ± 4° at 300 K that agrees very well with both the experimental tilt angle[1,2] of 30 ± 10° and an earlier computed tilt angle[32] of 25°. At 600 K, we observe an average tilt angle of 12 ± 5° (Figure 2). This is consistent with an earlier study of tilt angle, which found $\theta \approx 8°$ at very high temperature.[32] Figure 3a,b show snapshots of the equilibrium structures at 300 and 600 K, respectively. These results confirm the validity of the model and force fields to be used in our study of alkanethiols on NP surfaces.

3.2. Alkanethiol SAMs on Spherical NP Surfaces. *3.2.1. SAM Structure.* 3.2.1.1. Role of Temperature. We perform simulations of SAMs of alkanethiol homoligand surfactants with methyl tail groups on different sized gold NPs under various thermodynamics conditions to determine the role of curvature in the packing arrangement of molecules on spherical NP surfaces. Figure 4 shows snapshots of the equilibrium structures of 13-carbon alkanethiols at different temperatures on a gold NP of diameter 7 nm. At very high temperatures (900 and 600 K), we observe that the molecules do not order and point radially from the surface. As the temperature decreases, the alkanethiols tilt and order. We compute the center of mass (com)−com radial distribution functions (RDFs) at various temperatures (Figure 5). First and second peaks are observed at ∼4.85 and ∼8.6 Å, respectively, at all temperatures. In the low-temperature regime (≤450 K), the RDFs exhibit well-defined peaks suggesting long-range ordering of the molecules. With

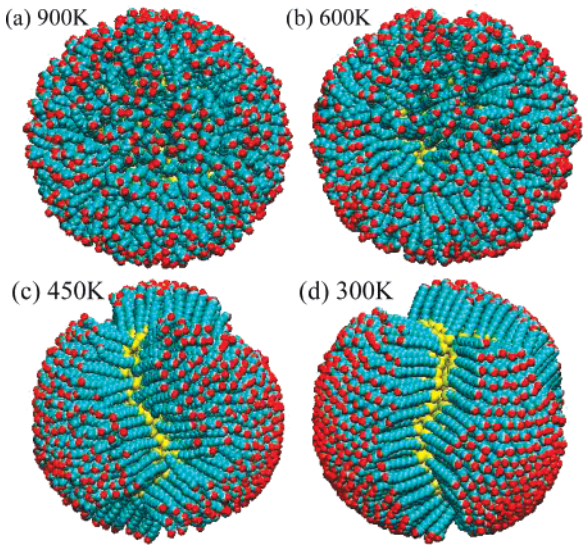

Figure 4. Snapshots of homoligand alkanethiol [SH−$(CH_2)_{13}$−CH_3] SAMs from our MD simulations at (a) 900, (b) 600, (c) 450, and (d) 300 K. Disclination lines arise due to the curvature of the surface.[36]

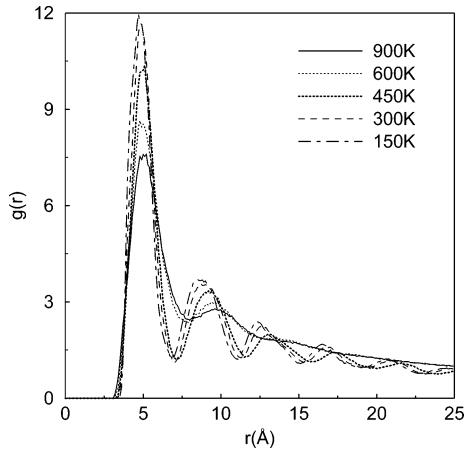

Figure 5. Center of mass pair correlation functions for the SH−$(CH_2)_{13}$−CH_3 molecule at different temperatures.

increasing temperature, the peak intensity at ∼4.85 and ∼8.6 Å decreases, and for $T > 600$ K, the peaks beyond 10.0 Å disappear. This shows the absence of long-range ordering in the high-temperature regime (above ∼600 K). Ordering appears only below ∼450 K. We further study this behavior in subsequent sections of this paper.

3.2.1.2. Role of Tail Length. We next study the dependence of the SAM structure on alkanethiol tail length. Figure 6 shows snapshots of the SAMs for different tail lengths at 300 K on a NP of diameter 7 nm. We see that as the carbon chain length increases, the molecular configuration changes from disordered to ordered and adopts an increasing tilt angle. There is a critical tail length (in this case 9-CH_2 groups) above which the ordering occurs. Both at low temperature (Figure 4) and for long surfactants (Figure 6), molecules group together with the same tilt angle. The structures of these separate regimes are similar to alkanethiols on a flat Au(111) surface. Hence, it appears that in the ordered phase the molecular arrangement on a spherical NP surface may be viewed as a collection of flat surface structures.

3.2.2. Head Group and Tail Group Spacing. 3.2.2.1. Role of Temperature and NP Size. To further elucidate the microscopic picture of surfactant self-assembly on spherical surfaces, we compute the head group and tail group spacing of alkanethiols

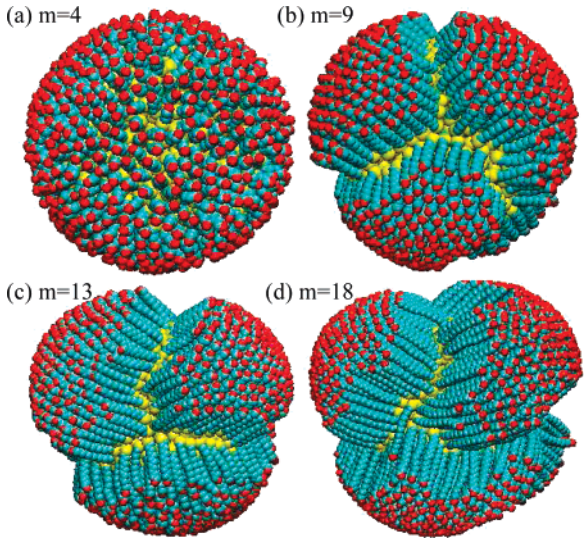

Figure 6. Snapshots of homoligand alkanethiol [SH−$(CH_2)_m$−CH_3] SAMs for different tail lengths; (a) $m = 4$, (b) $m = 9$, (c) $m = 13$, and (d) $m = 18$ at 300 K.

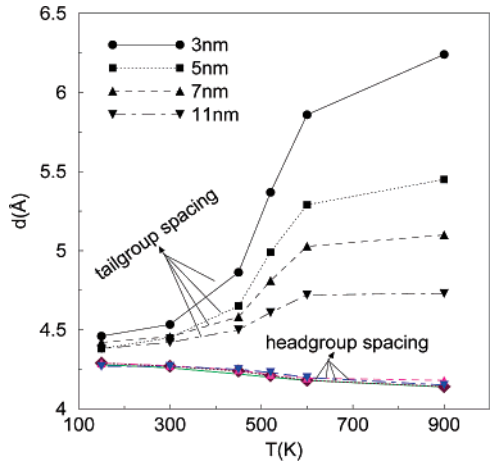

Figure 7. Sulfur head groups and methyl tail group spacing for SH−$(CH_2)_{13}$−CH_3.

on NP surfaces under various thermodynamic conditions. Figure 7 shows the spacing between the adjacent sulfur head groups and between the methyl tail groups on different sized NPs as a function of temperature. The spacing between the head group is defined as the smallest average distance between adjacent sulfur atoms. We find that the average head group spacing does not depend on NP size and decreases only slightly with temperature. The typical standard deviation of head group spacing on a single nanoparticle ranges from 0.15 to 0.25 Å depending on T. The average sulfur−sulfur spacings, ranging from 4.1 to 4.3 Å, are in agreement with experiment.[37]

The tail group spacing is computed by measuring the average smallest distance between two adjacent methyl groups (Figure 7). For all sizes of NPs studied, we find that the spacing between the methyl tail groups and the sulfur head groups are within 0.16 Å below 300 K. The spacing between the methyl tail groups is nearly constant for all NP sizes only at very low temperature (below 300 K). This was also observed by Jackson et al. in their recent experiment.[37] From Figure 7, we also see that unlike the head group spacing the spacing between the methyl tail groups differs for different NP sizes and increases significantly with T. At all T, the tail group spacing decreases with NP core diameter.

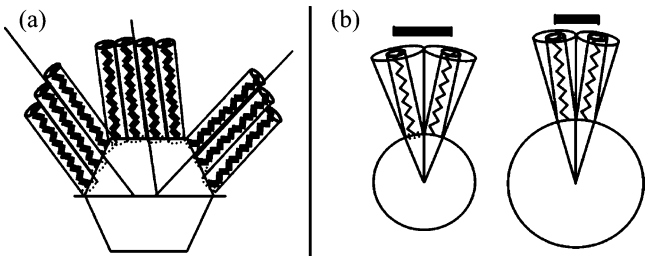

Figure 8. Schematic representations of an alkanethiol SAM on gold NP surfaces according to (a) crystallographic model[38] and (b) continuous model.[39] The figures are taken from ref 37.

To correlate the simulated tail group spacing to the actual packing arrangements of ligands on NP surfaces, we consider two models from the literature.

(i) Crystallographic model[38] (Figure 8a): According to this model, a Au nanocrystal's surface is composed of small (111) and (100) facets. Because locally these facets are flat, it may be assumed that SAMs of alkanethiols on these facets will be similar to that on flat surfaces. In this case, the tail group spacing should be equal to the head group spacing and should not depend on NP diameter.

(ii) Continuous model[39] (Figure 8b): In this model, the gold NP is considered as a perfect sphere. The sulfur head groups are tightly packed on the NP surface and the tail groups extend out radially from the surface. According to this model, the tail group spacing should decrease with increasing NP diameter and ultimately coincide with the head group spacing. The head group spacing should be independent of NP size.

Our results agree well with each of these models but in different temperature regimes. At low temperatures ($\lesssim$450 K), the tail group spacing is nearly independent of NP size (Figure 7) and is very close to the head group spacing. Hence, in the low-temperature regime, the equilibrium conformation of the ligand shell structure on NPs obeys the crystallographic model. In the high-temperature regime, for example at 900 K, the tail group spacing decreases with increasing NP size (Figure 7) and approaches the head group spacing. Hence, in the high-temperature regime the equilibrium conformation of the ligand shell structure obeys the continuous model. We note that gold NPs are faceted at sufficiently small sizes.[38] In our studies, though, the NPs are small; at high temperature the continuous model is valid due to the high mobility of the alkanethiols. At high temperature, the molecular kinetic energy is sufficiently high that the molecules can easily move over facet edges and hence the NP surface can be assumed as a perfect sphere.

3.2.2.2. Role of Tail Length. We next study the effect of carbon chain length on the head group and tail group spacing. Figure 9 shows the distributions of sulfur head group spacing on a sphere of diameter 7 nm at 300 K for different chain lengths. The head group spacing ranges from 3.45 to 7.0 Å, in good agreement with reported STM measurements of 3.5 to 7.0 Å.[37] We obtain an average head group spacing of 4.44 $\pm$ 0.52 Å compared to the experimental value of $\approx$5.0 Å. The average head group spacing observed in experiment is slightly higher than we observe (4.44 versus 5.0 Å). This slight difference may be due to a lack of statistical averaging in the scanning tunneling microscopy (STM) measurements where the number of measurements per nanoparticle diameter was less than 20, much fewer than we averaged in our simulations (typically, 70 000 independent runs). Because in the low-temperature regime the crystallographic model is valid, it is expected that the tail group spacing will not depend on the chain length, and this is indeed what we observe (not shown).

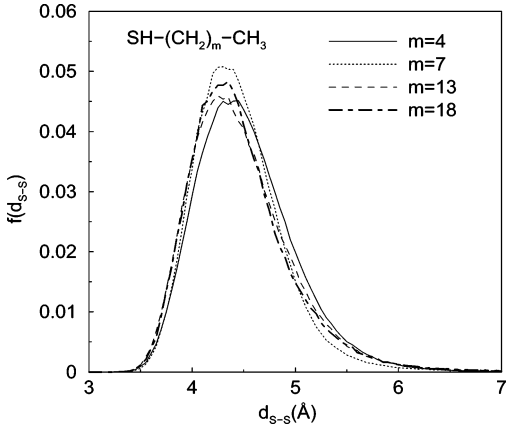

Figure 9. Probability distribution function of adjacent sulfur head group spacings for alkanethiols of various lengths.

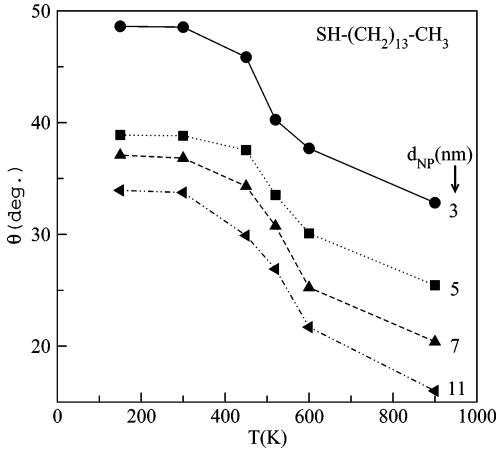

Figure 10. Variation of tilt angle θ for SH−$(CH_2)_{13}$−CH_3 alkanethiols as a function of temperature for different nanoparticle diameters (d_{NP}) and fixed tail length ($m = 13$).

3.2.3. Tilt Angle. There are several studies of the tilt structures of alkanethiol SAMs on flat gold surfaces.[1,2,32] We have already demonstrated that in the low-temperature regime, the tail group spacing of the alkanethiols on NP surfaces does not depend on molecular length. This indicates that the molecule is not perpendicular to the NP surface, but rather adopts a nonzero tilt angle. Figure 10 shows the variation of tilt angle θ for a 13-carbon alkanethiol system as a function of temperature for various nanoparticle core diameters d_{NP}. For all NP sizes, with increasing temperature the tilt angle initially decreases slowly and then rapidly to a lower value. It is known that[32] the tilt angle is determined by the competition between the potential energy and entropy contributions to the free energy. The potential energy contribution favors the tilting of the molecule whereas the entropy contribution favors zero tilting due to larger available volume for conformational changes. At high temperature, the entropic contribution to the free energy is larger than at low T due to the increased motion of the atoms near the chain ends. Hence, only a small tilt angle is seen at high temperature. The tilt angle depends strongly on NP size (Figure 10). At all temperatures, the tilt angle on small NPs is always larger than on large NPs, because the availability of more space for the alkanethiol tail on small NPs allows the molecule to adopt a larger tilt angle.

Many of the structural properties of alkanethiols on spherical NP surfaces depend on the ratio of tail length to NP size.[40] Because tilt angle increases with this ratio (Figure 10), an increase in tilt angle should occur with increasing tail length

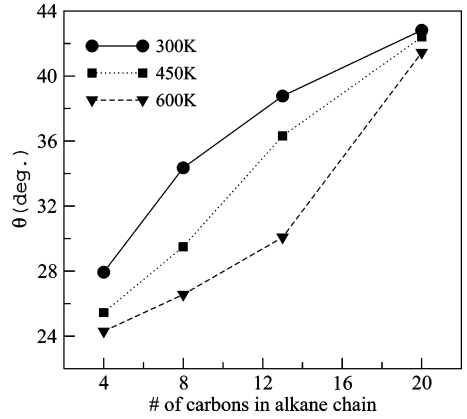

Figure 11. Tilt angle θ variation for SH−$(CH_2)_m$−CH_3 as a function of tail length at three different temperatures (600, 450, and 300 K) on a NP of diameter 5 nm.

for a fixed NP size. Figure 11 shows the variation of average tilt angle for different chain lengths on a sphere of diameter 5 nm at 300, 400, and 500 K. We indeed observe that the tilt angle increases rapidly with tail length, particularly at high temperature. It is expected that at very low temperature or for very long molecules (>20 CH_2 groups), the variation of tilt angle with chain length will be negligible due to decreased mobility of the alkanethiols on the NP surface.

4. Conclusions

Atomistic molecular dynamics simulations of homoligand alkanethiol SAMs have been carried out using a united atom model to investigate the molecular packing on NP surfaces as a function of temperature, molecular chain length, and nanoparticle size. Our studies predict a high-temperature regime in which the molecules on spherical surfaces orient randomly with respect to the surface normal with small tilt angle and exhibit no long-range order. As temperature decreases, the molecules adopt a significant tilt angle and exhibit long-range order. The equilibrium conformations of the ligand shell on spherical NP surfaces obey the crystallographic model in the low-temperature regime and the continuous model at high temperature. We further show that tilt angle depends strongly on the system temperature and the alkanethiol tail length. The major differences between homoligand alkanethiol SAMs on flat versus convex-curved surfaces may be summarized as follows: (i) homoligand surfactants on flat surfaces tilt mostly in any one particular direction (Figure 3) whereas on spherical surfaces a group of molecules tilt together (Figures 4 and 6) in various directions due to curvature induced disclinations; (ii) SAMs on flat surfaces always obey the crystallographic model whereas on spheres the crystallographic or continuous model is valid depending on temperature; (iii) at any given thermodynamic state points, the tilt angle for alkanethiols on NP surfaces is large compared to that on a flat surface; and (iv) SAMs on flat surfaces do not depend on the surface area of the substrate, but for spherical surfaces SAMs structure depends highly on the NP surface area.

Acknowledgment. We acknowledge financial support by the National Science Foundation (CTS-2004-0679-01), a joint grant with the Gubbins group at North Carolina State University. We thank F. Stellacci and A. M. Jackson for discussions regarding their experiments. S.C.G. thanks Keith Gubbins for many inspiring discussions on the subject of molecular simulation and surfactant self-assembly.

Note Added after ASAP Publication. This paper was published ASAP on October 4, 2007. The caption to Figure 11 was changed. The revised paper was reposted on October 5, 2007.

References and Notes

(1) Porter, M. D.; Bright, T. B.; Allara, D. L.; Chidsey, C. E. D. *J. Am. Chem. Soc*. **1987**, *109*, 3559.
(2) Nuzzo, R. G.; Dubois, L. H.; Allara, D. L. *J. Am. Chem. Soc*. **1990**, *112*, 558.
(3) Whitesides, G. M.; Laibinis, P. E. *Langmuir* **1990**, *6*, 87.
(4) Dubois, L. H.; Zegarski, B. R.; Nuzzo, R. G. *J. Am. Chem. Soc*. **1990**, *112*, 570.
(5) Evans, S. D.; Sharma, R.; Ulman, A. *Langmuir* **1991**, *7*, 156.
(6) Durand, R. R.; Bencosme, C. S.; Collman, J. P.; Anson, F. C. *J. Am. Chem. Soc*. **1983**, *105*, 2710.
(7) Chandross, M.; Grest, G. S.; Stevens, M. J. *Langmuir* **2002**, *18*, 8392.
(8) Malinsky, M. D.; Kelly, K. L.; Schatz, G. C.; Duyne, R. P. V. *J. Am. Chem. Soc*. **2001**, *123*, 1471.
(9) Thomas, K. G.; Kamat, P. V. *Acc. Chem. Res*. **2003**, *104*, 293.
(10) Collier, C. P.; Saykally, R. J.; Shiang, J. J.; Henrichs, S. E.; Heath, J. R. *Science* **1997**, *277*, 1978.
(11) Georganopoulou, D. G.; Chang, L.; Naam, J. M.; Thaxton, C. S.; Mufson, E. J.; Klein, W. L.; Markin, C. A. *Proc. Natl. Acad. Sci. U.S.A.* **2005**, *102*, 2273.
(12) Abbott, N. L.; Folkers, J. P.; Whitessides, G. M. *Science* **1992**, *257*, 1380.
(13) Frisbie, C. D.; Martin, J. R.; Duff, J. R. R.; Wrington, M. S. *J. Am. Chem. Soc*. **1992**, *114*, 7142.
(14) You, C. C.; De, M.; Han, G.; Rotello, V. M. *J. Am. Chem. Soc*. **2005**, *127*, 12873.
(15) You, C. C.; De, M.; Rotello, V. M. *Curr. Opin. Chem. Biol*. **2005**, *9*, *639*.
(16) Ulman, A. *An Introduction to Ultra-thin Organic films: From Langmuir-Blodgett to Self-Assembly*; Academic Press, Inc.: San Diego, CA, 1991.
(17) Collinson, M.; Bowden, E. F.; Taylor, M. J. *Langmuir* **1992**, *8*, 1247.
(18) Haussling, L.; Ringsdrof, H.; Schmitt, F. J.; Knoll, W. *Langmuir* **1991**, *7*, 1837.
(19) Shevchenko, E. V.; Talapin, D. V.; Kotov, N. A.; O'Brien, S.; Murray, B. C. *Nature* **2006**, *439*, 55.
(20) Andres, R. P.; Bielefeld, J. D.; Henderson, J. I.; Janes, D. B.; Kolagunta, V. R.; Kubiak, C. P.; Mahoney, W. J.; Osifchim, R. G. *Science* **1996**, *273*, 1690.
(21) Chen, S. W.; Ingram, R. S.; Hostetler, M. J.; Pietron, J. J.; Murray, R. W.; Schaaff, T. G.; Khoury, J. T.; Alvarez, M. M.; Whetten, R. L. *Science* **1998**, *280*, 2098.
(22) Fick, J. F.; Zamborini, F. P.; Osisek, A.; Murray, R. W. *J. Am. Chem. Soc*. **2001**, *123*, 7048.
(23) Lucarini, M.; Franchi, P.; Pedulli, G. F.; Gentilini, C.; Polizzi, S.; Pengo, P.; Scrimin, P.; Pasquato, L. *J. Am. Chem. Soc*. **2005**, *127*, 16384.
(24) Childsey, C. E. D. *Science* **1991**, *251*, 919.
(25) Gu, T.; Whitesell, J. K.; Fox, M. A. *J. Org. Chem*. **2004**, *69*, 4075.
(26) Ulman, A. *J. Mater. Educ*. **1989**, *11*, 205.
(27) Zhao, X.; Leng, Y.; Cummings, P. T. *Langmuir* **2006**, *22*, 4116.
(28) Jorgensen, W. L.; Madura, J. D.; Swenson, C. J. *J. Am. Chem. Soc*. **1984**, *106*, 6638.
(29) Jorgensen, W. L.; Maxwell, D. S.; Tirado-Rives, J. *J. Am. Chem. Soc*. **1996**, *118*, 11225.
(30) Hautman, J.; Klein, M. L. *J. Chem. Phys*. **1989**, *91*, 4994.
(31) Allen, M. P.; Tildesley, D. J. *Computer Simulation of Liquids*; Clarendon Press: Oxford, 1987.
(32) Vemparala, S.; Karki, B. B.; Kalia, R. K.; Nakano, A.; Vashisshta, P. *J. Chem. Phys*. **2004**, *121*, 4323. DeVries, G. A.; Brunnbauer, M.; Hu, Y.; et al. *Science* **2007**, *315*, 358−361.
(33) Mar, W.; Klein, M. L. *Langmuir* **1994**, *10*, 188.
(34) Majumder, C.; Briere, T. M.; Mizuseki, H.; Yoshiyuki. *J. Chem. Phys*. **2002**, *117*, 2819.
(35) Forester, T. R.; Smith, W. *The DL-POLY-2.13*; CCLRC, Daresbury Laboratory: Warrington, England, 1985.
(36) Nelson, D. R. *Nano Lett.* **2002**, *2*, 1125.
(37) Jackson, A. M.; Hu, Y.; Silva, P. J.; Stellacci, F. *J. Am. Chem. Soc*. **2006**, *128*, 11135.
(38) Zanchet, D.; Hall, B. D.; Ugarte, D. *J. Phys. Chem. B* **2000**, *104*, 11013.
(39) Landman, U.; Luedtke, W. D. *Faraday Discuss.* **2004**, *125*, 1.
(40) Singh, C.; Ghorai, P. K.; Horsch, M. A.; Jackson, A. M.; Stellacci, F.; Glotzer, S. C. submitted for publication.